Article

Shape-controlled hierarchical flowerlike Au nanostructure microarrays by electrochemical growth for SERS application

Lingling Zhang, Rui Hao, Dongjie Zhang, Hongjun You, Yanzhu Dai, Weihua Liu, and Jixiang Fang

Anal. Chem., **Just Accepted Manuscript** • DOI: 10.1021/acs.analchem.0c01333 • Publication Date (Web): 16 Jun 2020

Shape-controlled hierarchical flowerlike Au nanostructure microarrays by electrochemical growth for SERS application

Lingling Zhang,[†] Rui Hao,[†] Dongjie Zhang,[†] Hongjun You,[‡,*] Yanzhu Dai,[§] Weihua Liu,[†] Jixiang Fang [†,*]

[†]School of Electronic Science and Engineering, Faculty of Electronic and Information Engineering, Xi'an Jiaotong University, Xi'an, Shaanxi, 710049, China
[‡]School of Science, Xi'an Jiaotong University, Xi'an, Shaanxi, 710049, China
[§]School of Microelectronics, Faculty of Electronic and Information Engineering, Xi'an Jiaotong University, Xi'an, Shaanxi, 710049, China
[*]To whom correspondence should be addressed. E-mail: jxfang@mail.xjtu.edu.cn (J.F.), hjyou@mail.xjtu.edu.cn (H.Y.)

ABSTRACT: How to fabricate Au nanostructures conveniently on micro/nanostructured arrays surface with low cost has become a crucial and urgent challenge. In this study, we demonstrate hierarchical flowerlike Au nanostructures with rich nano thorns (HF-AuNTs) through one-step electrochemical deposition. The morphology of the HF-AuNTs is easily manipulated via controlling applied potential or precursor solution concentration of electrodeposition. The as-prepared HF-AuNTs possessing unique local morphology of thin petals and dense thorns, are further applied in the Si micro-pit arrays to acquire HF-AuNTs microarrays. As an initial detection, these HF-AuNTs microarrays exhibit a fascinating surface enhanced Raman spectroscopy (SERS) consistency (relative standard deviation, RSD=7.17%) and sensitivity with the limitation of crystal violet (CV) reaching to 10^{-10} M, and rhodamine 6G (R6G) reaching to 10^{-11} M. The HF-AuNTs microarrays with well-defined shape and elaborate structure may be applicated in SERS substrates, superhydrophobic materials, and so on.

Micro/nanostructured arrays have attracted great interests and were widely applied in catalysis,[1] electronics,[2] sensors[3,4] and surface-enhanced Raman scattering (SERS),[5,6] due to their microscale periodicity and nanostructured building blocks. Generally, the fabrication of the micro/nanostructured arrays as SERS substrates is based on two main processes: micro/nanostructured arrays preparation and metal nanomaterials deposition.[7,8] In nature, the SERS performance are dominated by well-engineered micro/nanostructured arrays and morphology-controlled metal nanostructures on the arrays surface, both of which are interdependent for final morphology of substrates and crucial to the distribution and quality of hot spots.[4,6] So, multitudinous approaches to micro/nanostructured arrays for SERS detection have been widely developed in order to improve SERS ability in practical application.[9,10] After a long-term development, the methods to prepare the micro/nanostructured arrays, including the lithography,[11,12] template-based[13,14] and invisible template[15] techniques, are well-studied and fairly mature. Up to now, various micro/nanostructured arrays with adjustable separation distance and size dimension have been reported, such as nanopillar,[16] nanorod,[17] nanowires,[13,18] raster,[11] bowtie,[19] and nanograss.[20]

However, the metal nanomaterials deposition still heavily depends on the magnetron sputtering and electron beam evaporation,[21,22] which are used just to generate single shape of spherical particles, cannot achieve the regulate and control of morphologies.[23,24] As known, the intrinsic chemical and physical properties of nanomaterials are strongly determined by their shape.[25,26] Recently, the electrodeposition method has been used as an effective way to control the structures and morphologies of the as-deposited nanomaterials.[27,28] Compared to other well-developed synthetic methods, the electrochemical deposition makes it more convenient, and easier to prepare different nanostructures on conducting substrates,[29] which provides more probabilities for the design and construction of SERS substrates.[30] Meanwhile, the final structures of nanomaterials directly deposited on an electrode surface and the growth rate can be readily and independently controlled by precisely-adjusting the interplay between the rate of crystal growth and mass transport.[31] Although there are some strategies of synthesizing Ag and Pt nanomaterial by electrodeposition, several reported Au nanostructures on micro/nanostructured arrays surface are mainly Au dendrites or flowers with sparse branches and stout petals, lacking the micro-structure.[15,32] It has been verified that the narrow gaps between sharp corners or edges of the nanostructured noble metals, so-called "hot spots", are essential for exciting the localized surface plasmons,[33,34] thus the Au nanomaterials with robust morphology will go against the SERS performance. Therefore, it is particularly important to realize morphological control of Au nanomaterials with micro-refined structures on the pattern array surface.

In this study, we demonstrated the hierarchical flowerlike Au nanothorns (HF-AuNTs) with abundant petal-shaped Au nanosheets or nanopricks as building blocks on the microarrays surface, through electrochemical deposition technique that was simple and easily controlled. Here, the effects of the experimental parameters, including deposition potential, concentration, and time, have been successively

discussed. We prepared HF-AuNTs on the FTO, silicon wafer with Au covered or microarrays and compared the SERS performances of the as-obtained substrates. The HF-AuNTs microarrays revealed splendid size homogenous and outstanding SERS performance. The test results showed that the HF-AuNTs microarrays would be an effective platform for SERS detection with highly sensitivity and reproducibility.

EXPERIMENTAL SECTION

Electrochemical preparation of HF-AuNTs. Fluorine doped tin oxide on the glass (FTO) electrode (0.8 cm × 3.5 cm) was used as a working electrode. Before electrochemical deposition, the FTO substrates were washed by ultrasonic cleaning for 15 min each in acetone, ethanol, and deionized water, respectively. Then cleaned FTO substrates were dried by N_2 gas and kept in drying chamber. After that, the FTO electrode was immersed in a certain concentration $HAuCl_4$ and HCl electrolyte. In this work, the electrochemical deposition of hierarchical flowerlike Au nanothrons (HF-AuNTs) was performed in a double-electrode system with constant potential electrolysis. The FTO substrate was connected to the cathode and the carbon rod was connected to the anode to control the external electric field. After deposition, the FTO electrodes were thoroughly washed with deionized water and dried in air.

Fabrication of HF-AuNTs on Si substrates with gold covered (Si-Au). For the Si substrates with gold covered, a gold layer (50 nm in thickness) was deposited on the Si substrates by an electron beam evaporation (EBE, TF500). The thickness of the gold layer can be adjusted by changing the evaporation current and time, and the value is estimated for the data provided by the instruction manual of the sputter coater. Then, the Si substrate with gold covered (Si-Au) was cut into 0.8 cm × 3.5 cm, and used as electrode to grow HF-AuNTs. The electrochemical deposition of HF-AuNTs on the Si-Au electrode was the same as that on the FTO electrode.

Fabrication of HF-AuNTs on Si micron-pit (MP) arrays. For the synthesis of Si-MP arrays. n-Type (100) Si wafers were coated with layers of negative photoresist (RPN-1150) approximately 3 μm thick and cured at 90 °C for 90 s. The photoresist was then exposed using a lithography tool (URE_2000S) and the unexposed photoresist was then removed using developer (RZX-3038). Then the wafer with leaving nearly-circular-shape photoresist hole on the surface was dried at 110 °C for 13 min. The etcher was operated under inductively coupled plasma (ICP, ICP-2C) at a pressure of 3×10^{-3} Pa, and coil and platen powers of 300 W and 70 W, respectively. Each cycle of etching (with SF_6) and passivation (with C_4F_8) was 30 s and 35 s, respectively. The cycle of etching and passivation was 6 times. The flow rates for SF_6 and C_4F_8 were both 30 sccm. Thereafter, the leaving photoresist was removed in acetone and the final wafer with micro-pit arrays was washed with deionized water, dried by N_2 gas and kept in drying chamber. Then, the Si substrate with micro-pit arrays was cut into 0.8 cm × 3.5 cm, and used as electrode to grow HF-AuNTs. The electrochemical deposition of HF-AuNTs on the Si-MP array electrode was the same as that on the FTO electrode.

RESULT and DISCUSSION

Figure 1 schematically illustrated the main fabrication process of the microarrays of HF-AuNTs. First, the photoresist was prepared as the micro-pit array template by a UV lithography technique.[11] Then, by following the inductively coupled plasma (ICP) etching process[20] and removing the photoresist template, the highly uniform Si-MP arrays were obtained. After that, the regular array of HF-AuNTs was synthesized by further electrochemical deposition on the as-formed Si-MP array surface. Finally, the as-prepared microarray of HF-AuNTs was used as an active SERS substrate. The manufacture of Si-MP array was proficient and widely reported. Here, we mainly focused on the electrochemical deposition of HF-AuNTs.

Fabrication and characterization of HF-AuNTs. At the beginning, in order to simplify the experiment model, we chose the fluorine doped tin oxide (FTO) glass electrode as the no-array substrate to study the growth law of HF-AuNTs by electrodeposition. During the electrolysis process, the reduction of $HAuCl_4$ to form Au (0) was always expected to occur for growing specific structures.[35] For a typical synthesis, the HF-AuNTs were grown on FTO electrode surface, in an aqueous solution containing 10 mM of $HAuCl_4$ and 0.5 M hydrochloric acid (HCl) aqueous solution. The chronoamperometry technique action was employed for electrochemical deposition of HF-AuNTs with the potential at -1.0 V and deposition time of 30 min. Afterwards, the electrodes were washed with water and dried at room temperature. As shown in Figure 2a, the low magnification scanning electron microscopy (SEM) image showed a lot of highly monodisperse Au nanostructures electrodeposited throughout the FTO electrode surface with flower-like shape and an average diameter of particles around 5 μm. Furthermore, high magnification SEM images (Figure 2b and c) revealed the detail of the HF-AuNTs. The flower-like Au microstructure was constructed by many thin "petals" combined in a staggered way. Interestingly, there were many nanothorns on the top and sides extended outward of petals, which were much different from that on the reported flower-like Au nanostructures whose petals with smooth edges were stout and massive.[31,36] The surface planes of the HF-AuNTs were investigated by the X-ray diffraction (XRD). As shown in Figure 2d, the ratios of the intensities at the diffraction peaks due to the (111) plane relative to the (200) and (220) planes were 3.1 and 6.9, respectively; these values are significantly greater than those (1.9 and 3.1, respectively) commonly obtained for polyAu (JCPDS 04-0784).[36] These observations suggest that the (111) plane was the predominant orientation in the HF-AuNTs. The energy dispersive X-ray (EDX) spectrogram was used to record and analyse the elemental composition of the HF-AuNTs. The spectrogram of the EDX measurement illustrated that the characteristic peaks of the Au (Figure S1). Furthermore, the X-ray photoelectron spectroscopy (XPS) characterization was shown in Figure S2. Consistent with EDX result, XPS data indicated that there was only Au element on the FTO substrate. the peaks of Au 4f were located at 84.2 eV and 87.9 eV, matching with the standard binding energies of Au $4f_{7/2}$ (84.0 eV) and Au $4f_{5/2}$ (87.7 eV). These results revealed the high purity of HF-AuNTs.

Effects and growth mechanism of the experimental parameters. Through choosing the appropriate electrolyte, deposition voltage and duration, various Au nanomaterials can be synthesized. The anisotropic growth of noble-metal nanostructures in the electrodeposition system have been deeply studied in the previous reports. The hierarchical morphology of deposited noble-metal nanostructures is usually

determined by following factors: limited diffusion of metal ions near the electrode, concentration field and electric field near the electrode, and limited diffusion of metal atoms on the disposition crystalline plane. The concentration of metal ions near the tips of hierarchical nanostructure is higher,[37] that induced the protuberant growth.[38] The electric field would limit the diffusion of metal ions and directed the growth of nanostructures along the electric field directions.[38,39] To further understand the influence factors of the growth of Au nanostructures, different electrodeposition parameters were investigated, including deposition potential, and concentrations of HCl and $HAuCl_4$. As we know, the morphology of Au nanostructures strongly depended on the deposition potential by using electrodeposition method.[28] Therefore, the applied potential on Au nanostructures was first explored ranging from -0.25 V to -1.5 V. Different sizes and morphologies of Au nanostructures were obtained by using different potentials in 0.5 M HCl and 10 mM $HAuCl_4$ for 30 min.

As the potential jumped from -0.25 V to -1.5 V (Figure 3a-f), the Au nanostructures ranged from irregular spherical shape (Figure 3a) to hierarchical flower-like one (Figure 3b-f), while the crystal density increased with the potential negative shift. Interestingly, the petals on hierarchical flower-like Au nanostructures were firstly changed from thick slice (Figure 3b) to thin slice (Figure 3c-e) and then to cubic prism (Figure 3f). It should be noted that hierarchical flowerlike Au nanostructures with many thin nanothorns (HF-AuNTs) were obtained when the potential was -1.0 V (Figure 3d). In the electrodeposition growth system, with the increase of electric potential, the direction functions of electric field became strong for the anisotropic growth of Au nanostructures. Thus, from 0 V to -1.0 V, with the increase of negative potential, the nanothorns of Au nanostructure become thin and sharp. When the potential further increase, the H_2O molecules will be electrolyzed into H_2 and O_2. The standard potential for electrolyzation of H_2O is -1.23 V. In our system, the aqueous solution is acidic, indicating that the electrolyzation potential would be less than -1.23 V. When the potential increase more than -1.0 V, to -1.5 V, the electrolyzation reaction of H_2O would happen on the surface of Au nanostructures. The deposition velocity would be decreased, and Au ions and Au atoms have more times to diffusion. The anisotropic growth would be limited. Thus, those nano-brambly surface topography of each petals disappeared and the nanothorns would become cubic prism. Therefore, to synthesize shape-controlled and well-defined Au nanostructures, -1.0 V was chosen in the following experiment.

In addition, the concentration of HCl and $HAuCl_4$ were investigated to explain growth process of Au nanostructures. Figure S3 showed the SEM images of Au nanostructures formed on FTO surfaces at -1.0 V for 30 min with 10 mM $HAuCl_4$ and different concentration of HCl solution ranging from 0 to 1 M. As displayed in Figure S3a, in the absence of HCl, the Au deposits contained a lot of popcorn-like particles, without any flower-like Au nanostructures, indicating that HCl had a significant impact on the growth of the hierarchical flower-like Au nanostructures. The flower-like Au nanostructures with brawny thorns appeared on the lower concentration of HCl (0.1 M, Figure S3b). Furthermore, the thinner petals and slender thorns on the flower-like Au nanostructures were obtained when the concentration of HCl was 0.5 M (Figure S3c). As researchers had shown that the impact of the HCl on the anisotropic gold nanostructures mainly included two functions: on the one hand, the Au^{3+} united Cl^- to form the complex of $AuCl_4^-$, which influenced the reduction kinetics of Au^{3+} in the electrodeposition;[40-42] on the other hand, Cl^- probably adsorbed onto (111) facet on the surface of Au nanoparticles.[31] The purposeful distribution of Cl^- on certain crystal planes had straightforward effects on the anisotropic growth of the Au crystals, as demonstrated by the shape-controlled of Au using Cl^- in many previous reports.[43,44] If the concentration of HCl increased to 1.0 M (Figure S3d), petals grew bigger and rougher thorns were observed. However, the density and coverage of flower-like Au nanostructures on FTO electrode substrates obviously decreased. Thus, the increase of HCl concentration had negative effect on gold nanostructure growth and fractal, which might result from inhibiting effect of Cl^- on the reduction of $AuCl_4^-$ to gold.[27] Based on the above results, 0.5 M was chosen as the optimal HCl concentration.

Interestingly, the products contain heavily aggregated Au particles with irregular shapes in the control experiments of replacing HCl with sulfuric acid (H_2SO_4) or acetic acid (CH_3COOH), where all other experimental conditions were kept the same (Figure S4). The failure to obtain urchin-like Au arrays in the absence of HCl indicated that HCl had a critical impact on the growth of the HF-AuNTs. It was known that the synthesis of hierarchical Au nanostructures was indeed diffusion-limited growth. Thus, HCl was used as a shape-directing agent, which was adsorbed on the surface of the Au crystals and changed nucleation and growth rates, to control the formation of HF-AuNTs.

Figure S5 showed the morphological evolution of the HF-AuNTs at -1.0 V in 0.5 M HCl and varying $HAuCl_4$ concentration. The diameter of gold nanostructure increased from ~ 1μm to ~ 5 μm with the concentration of $HAuCl_4$ increasing from 1 mM to 15 mM (Figure S5a-d). Moreover, the morphology of gold nanostructures was gradually prone to hierarchical flower-like Au nanothorns (Figure S5b-c) from simple Au nanothorns (Figure S5a), when $HAuCl_4$ concentration increased. It was noted that if $HAuCl_4$ concentration was over 10 mM, the thickness of the petals on gold nanostructures increased and the size of gold nanostructures grew bigger accordingly (Figure S5d). Consequently, the well-defined HF-AuNTs were obtained when the precursor concentration was 10 mM.

The electrodeposition time was also investigated to control the synthesis of the HF-AuNTs. Figure S6 showed the representative SEM images of the Au nanostructures prepared with different electrodeposition time. When the deposition time was 1 min, there were only litchi-like spherical Au nanoparticles with small size and little bumps on the FTO electrode surface. (Figure S6a). As time went by, the Au nanostructures grew bigger and possessed more complicated thorns (Figure S6b-d), but the quantity of Au nanostructures at different stages on the FTO surface was almost the same. It should be concluded that the nucleation of HF-AuNTs quickly occurred in the initial phase (maybe less than 1 min, Figure S6a), after which process of growth became dominant.[45] Firstly, a large quantity of Au atoms were formed by fast reduction of $AuCl_4^-$ with the constant potential of -1.0 V. Then, plenty of Au nuclei were distributed randomly on the FTO electrode surface. Meanwhile, Cl^- was preferentially adsorbed on the specific Au crystal planes by self-assembly, which prevented the new generation of Au atoms or clusters

from further aggregation.[45] Moreover, the adsorbed Cl^- broke the equilibrium of the system and acted as a shape-directing agent for initial branching, which benefited to the deposition of Au crystals on the original nuclei and coalescence of the neighbouring ones at the tips and stems of the short petals, followed by full growth of the HF-AuNTs.

SERS performance of HF-AuNTs on the FTO substrate. The as-synthesized HF-AuNTs possessed exposed thin-petals and abundant nanothorns, which made it easier to adsorb more molecules and enhanced electromagnetic field (EMF).[46] More importantly, the blank HF-AuNTs on the FTO electrode surface did not present any Raman signal (Figure S7), which gave a "clean" Raman background for further test. In this case, the HF-AuNTs were expected as SERS substrates. Four typical gold nanostructures, spherical Au nanoparticles (S-AuNPs, -0.25V, Figure 3a), hierarchical flowerlike Au thick-pieces (HF-AuTPs, -0.5V Figure 3b), HF-AuNTs (-1.0 V, Figure 3d) and hierarchical flowerlike Au shout-prisms (HF-AuSPs, -1.5V, Figure 3f) were selected for SERS detection. The SERS performances of the as-fabricated Au nanostructures were investigated using 10^{-7} M crystal violet (CV) as probe molecules with a laser at excitation wavelength of 785 nm, and laser spot of ~20 μm in diameter (under 100 × objective). Figure 4a showed the SERS spectra of CV collected on these Au nanostructures, and the main vibrational peaks of CV molecules were located at 727, 808, 916, 1173, 1388, 1532, 1587, and 1617 cm^{-1}. The characteristic peak intensities of the spectra at 1173 and 1617 cm^{-1} were shown in Figure 4b. It could be seen that the SERS performance was sensitive to the morphology of Au nanostructures and the HF-AuNTs showed the best SERS performance. Moreover, the UV-vis absorption spectra were shown in Figure S8. Compared with the FTO substrate, the HF-Au NTs did not exhibit any distinct absorption band. We investigated the SERS performance of HF-AuNTs on the Si-MP array surface under the laser irradiation with wavelengths of 532 and 633 nm (Figure S9). The SERS spectra of CV from HF-AuNTs under 785 nm laser irradiation strengthened than that under 633 or 532 nm laser irradiation.

Fabrication and SERS performance of HF-AuNTs on Si-Au and Si-MP array. To judge the reproducibility of the electrodeposition approach, four samples were prepared on the FTO substrates under the same condition. As shown in Figure S10a-d, these four samples possessed the semblable nanostructure with thinner petals and slender thorns. Figure S11 exhibited the Raman spectra of CV at 10^{-8} M from the reproduced four HF-AuNTs samples. For comparison, the SERS intensities at 1173 cm^{-1} from these four HF-AuNTs substrates were shown in Figure S12, which demonstrated the uniform consistency of these samples.

Sensitivity and reproducibility are significant for the practical application of SERS substrates.[47] Compared to the other three different Au nanostructures, the HF-AuNTs possessed the precise micro-region, which was beneficial to the sensitivity. Unfortunately, the HF-AuNTs on the FTO were uneven in size and distribution, thus possibly going against the reproducibility. Here we chose two methods to improve the dimensional uniformity, and then enhanced the signal consistency of SERS performance.

Firstly, we deposited the Au film on the silicon wafer (Au-Si, Figure 5a) and synthesized the HF-AuNTs by electrochemical deposition. Hundreds of Au nanoparticles were closely ranged on the silicon wafer surface, providing sufficient nucleation sites for HF-AuNTs fabrication. It could be seen from the above results that the electrodeposition potential was the most critical influence on the morphology of Au nanostructure. Hence, we chose different electrodeposition potentials (-0.5 V, -1.0 V, -1.5V) with 0.5 M HCl and 10 mM $HAuCl_4$, to control the synthesis of HF-AuNTs on the Au-Si electrode surface (Figure 5b-d). As shown in the SEM pictures, various hierarchical Au nanostructures were densely distributed on the Si-Au surface with uniform shape and size.

Secondly, we utilized the silicon micron-pit (MP) arrays to obtain the regularly-growing HF-AuNTs. After inductively coupled plasma (ICP) etching and removing of photoresist mask, ~15 μm wide and ~3 μm depth MP had been achieved with a space of ~10 μm (Figure 6a-b). The etched edges and bottoms of the MP array were not smooth as the unetched silicon wafer, which supplied favourable conditions to form HF-AuNTs. Similarly, different electrodeposition potentials (-0.5 V, -1.0 V, -1.5V) were used to synthesis the HF-AuNTs on the silicon micropatterns surface in 0.5 M HCl and 10 mM $HAuCl_4$. Figure 6c-e revealed that the HF-AuNTs were mainly generated on the edges of the MP array and displayed the proximate tendency to that on FTO surface (Figure 3b, d, f). Meanwhile, some initial HF-AuNTs appeared at the bottoms of the array, because of the relative inferior nucleation locations. The MP array furnished the three-dimensional (3D) distribution of HF-AuNTs. Figure 6f demonstrated that with a longer deposition time, the HF-AuNTs became serried and closely interwoven from the MP edges.

The most refined HF-AuNTs on FTO (Figure 3d), Si-Au (Figure 5c) and Si-MP array (Figure 6f) under similar electrodeposition condition were chosen to evaluate the SERS reproducibility quantitatively. Figure 7a-c revealed the SERS spectra of CV molecule with 10^{-7} M concentration from the HF-AuNTs on FTO, Si-Au, and Si-MP array, respectively. We calculated the relative standard deviation (RSD, the ratio of standard deviation to the mean) of characteristic peaks (1173 cm^{-1}) intensity from forty spectra on Figure 7a-c. As shown in Figure 7d, the RSD of FTO substrate reached 12.74%, which was 2.2 times of that from the Si-Au substrate (5.85%) and 2.0 times of that from Si-MP array substrate (6.29%). Meanwhile, the HF-AuNTs on Si-MP array substrate (HF-AuNTs microarrays in short) possessed much higher SERS signal intensity than that on the FTO substrate or Si-Au substrate. The gold cover or MP arrays on the silicon wafer facilitated the evenly distributed nucleation of HF-AuNTs, thus enhancing the signal consistency. Furthermore, the micromap of SERS intensity from the HF-AuNTs microarrays substrate was shown in Figure 7g, corresponding with the SEM image (Figure 7e) and optical microscope image (Figure 7f, white dotted box). Herein, the strongest signal intensity mainly distributed in the edges of the micro-pits, where generated abundant HF-AuNTs. Besides, the Au nanostructures on the bottom of the micro-pits, as shown in Figure 6f and 7e, contributed the stronger signal intensity. And interestingly, the SERS intensity on the intersection of four micro-pits was relatively lower, because there was vacant with Au nanostructures (Figure 7e). This SERS micromap not only reflected the 2D array pattern but also revealed the exquisite signal consistency in micro-refined region. In this work, the ordered MP arrays constructed subsistent "hot spot" in the whole 3D space, which were more suitable to catch detection molecule and leaded to an increase in the Raman signal intensity.[48-50] Especially, the RSD of signal intensity on Si-MP

array substrate was better than the results of similar ordered array system deposited with Au film reported before.[31]

In addition, to evaluate the SERS sensitivity HF-AuNTs microarrays, the Raman spectra of CV with different concentrations (from 10^{-7} to 10^{-11} M) were shown in Figure 8a. Additionally, the characteristic band of CV at 1173 cm^{-1} was used as a quantitative peak to evaluate the SERS sensitivity. It was revealed that the characteristic peak of CV at 1173 cm^{-1} could be clearly identified even at a very low concentration of 10^{-10} M, exhibiting an excellent detectability. Besides, the Raman spectra of rhodamine 6G (R6G) with different concentrations (from 10^{-7} to 10^{-12} M) were shown in Figure 8b, and the detection limit of R6G was 10^{-11} M, which was better than many reports.[22,51] Moreover, the Figure 8c presents the SERS spectra of thiram with different concentrations from the HF-AuNTs microarrays. The characteristic peak at 1380 cm^{-1} was still identified even when the concentration was decreased to 10^{-9} M, which was lower than previous report.[52] Judging from the above results, it could be ratiocinated that the HF-AuNTs exhibited great potential in practical applications with preferable sensitivity and excellent reproducibility.

CONCLUSION

In this work, shape-controlled and well-defined hierarchical flowerlike Au nanothorns have been synthesized using a simple and one-step electrodeposition method. The size and morphology of Au nanostructures were successfully regulated by changing electrodeposition conditions, such as deposition potential, deposition time, and solution concentrations of HCl and $HAuCl_4$. The HF-AuNTs on the FTO, Si-Au, and Si-MP array substrates were selected to study the sensitivity and reproducibility of SERS signals. Furthermore, the HF-AuNTs microarrays showed splendid SERS performance and consequently had a potential application in biological and chemical molecules detection.

ASSOCIATED CONTENT

Supporting Information

Some of Experimental section (Material, SERS measurement, Characterization), characterization data from SEM, XPS, EDS and UV-visible spectra, effects of electrodeposition parameters, results reproducibility (PDF).

AUTHOR INFORMATION

Corresponding Author

*E-mail: jxfang@mail.xjtu.edu.cn (J.F.), hjyou@mail.xjtu.edu.cn (H.Y.)

Notes

The authors declare no competing financial interest.

ACKNOWLEDGMENT

This work was supported by the programs supported by the National Natural Science Foundation of China (No. 21675122 and 21874104), Shaanxi Province Key Industries Innovation Chain Project (2019ZDLSF07-08), Basic Public Welfare Research Project of Zhejiang Province (No. LY20E010007), Natural Science Foundation of Shaanxi Province (No. 2019JLP-19), the World-Class Universities (Disciplines), the Characteristic Development Guidance Funds for the Central Universities, and the Fundamental Research Funds for the Central Universities. The characterizations of materials are supported by Instrument Analysis Center of Xi'an Jiaotong University.

REFERENCES

(1) Zhao, D.; He, Z.; Wang, G.; Wang, H.; Zhang, Q.; Li, Y. A novel efficient ZnO/Zn(OH)F nanofiber arrays-based versatile microfluidic system for the applications of photocatalysis and histidine-rich protein separation. *Sensors Actuat. B-Chem.* **2016**, *229*, 281-287.

(2) Wang, Y.; Zhang, M.; Lai, Y.; Chi, L. Advanced colloidal lithography: From patterning to applications. *Nano Today* **2018**, *22*, 36-61.

(3) Zhou, M.; Xu, Y.; Lei, Y. Heterogeneous nanostructure array for electrochemical energy conversion and storage. *Nano Today* **2018**, *20*, 33-57.

(4) Cheng, Z.; Zhang, D.; Lv, T.; Lai, H.; Zhang, E.; Kang, H.; Wang, Y.; Liu, P.; Liu, Y.; Du, Y.; Dou, S.; Jiang, L. Superhydrophobic Shape Memory Polymer Arrays with Switchable Isotropic/Anisotropic Wetting. *Adv. Funct. Mater.* **2018**, *28*, 1705002.

(5) Liu, B.; Chen, S.; Zhang, J.; Yao, X.; Zhong, J.; Lin, H.; Huang, T.; Yang, Z.; Zhu, J.; Liu, S.; Lienau, C.; Wang, L.; Ren, B. A Plasmonic Sensor Array with Ultrahigh Figures of Merit and Resonance Linewidths down to 3 nm. *Adv. Mater.* **2018**, *30*, e1706031.

(6) Chirumamilla, M.; Toma, A.; Gopalakrishnan, A.; Das, G.; Zaccaria, R. P.; Krahne, R.; Rondanina, E.; Leoncini, M.; Liberale, C.; De Angelis, F.; Di Fabrizio, E. 3D nanostar dimers with a sub-10-nm gap for single-/few-molecule surface-enhanced raman scattering. *Adv. Mater.* **2014**, *26*, 2353-2358.

(7) Wang, J.; Duan, G.; Liu, G.; Li, Y.; Xu, L.; Cai, W. Fabrication of gold and silver hierarchically micro/nanostructured arrays by localized electrocrystallization for application as SERS substrates. *J. Mater. Chem. C* **2015**, *3*, 5709-5714.

(8) Li, X.; Chen, G.; Yang, L.; Jin, Z.; Liu, J. Multifunctional Au-Coated TiO2 Nanotube Arrays as Recyclable SERS Substrates for Multifold Organic Pollutants Detection. *Adv. Funct. Mater.* **2010**, *20*, 2815-2824.

(9) Kravets, V. G.; Kabashin, A. V.; Barnes, W. L.; Grigorenko, A. N. Plasmonic Surface Lattice Resonances: A Review of Properties and Applications. *Chem. Rev.* **2018**, *118*, 5912-5951.

(10) Shi, R.; Liu, X.; Ying, Y. *J.* Facing Challenges in Real-Life Application of Surface-Enhanced Raman Scattering: Design and Nanofabrication of Surface-Enhanced Raman Scattering Substrates for Rapid Field Test of Food Contaminants. *Agr. Food Chem.* **2018**, *66*, 6525-6543.

(11) Ji, R.; Lee, W.; Scholz, R.; Gösele, U.; Nielsch, K. Templated Fabrication of Nanowire and Nanoring Arrays Based on Interference Lithography and Electrochemical Deposition. *Adv. Mater.* **2006**, *18*, 2593-2596.

(12) Zhang, J.; Yang, B. Patterning Colloidal Crystals and Nanostructure Arrays by Soft Lithography. *Adv. Funct. Mater.* **2010**, *20*, 3411-3424.

(13) Huang, Z.; Fang, H.; Zhu, J. Fabrication of Silicon Nanowire Arrays with Controlled Diameter, Length, and Density. *Adv. Mater.* **2007**, *19*, 744-748.

(14) Li, Y.; Zhang, J.; Zhu, S.; Dong, H.; Jia, F.; Wang, Z.; Sun, Z.; Zhang, L.; Li, Y.; Li, H.; Xu, W.; Yang, B. Biomimetic Surfaces for High-Performance Optics. *Adv. Mater.* **2009**, NA-NA.

(15) Wang, J.; Duan, G.; Li, Y.; Liu, G.; Dai, Z.; Zhang, H.; Cai, W. An invisible template method toward gold regular arrays of nanoflowers by electrodeposition. *Langmuir* **2013**, *29*, 3512-3517.

(16) Yang, S.; Cai, W.; Yang, J.; Zeng, H. General and simple route to micro/nanostructured hollow-sphere arrays based on electrophoresis of colloids induced by laser ablation in liquid. *Langmuir* **2009**, *25*, 8287-8291.

(17) Lin, H.; Cheung, H.-Y.; Xiu, F.; Wang, F.; Yip, S.; Han, N.; Hung, T.; Zhou, J.; Ho, J. C.; Wong, C.-Y. Developing controllable anisotropic wet etching to achieve silicon nanorods, nanopencils and nanocones for efficient photon trapping. *J. Mater. Chem. A* **2013**, *1*, 9942.

(18) Weisse, J. M.; Kim, D. R.; Lee, C. H.; Zheng, X. Vertical Transfer of Uniform Silicon Nanowire Arrays via Crack Formation. *Nano Lett.* **2011**, *11*, 1300-1305.

(19) Roxworthy, B. J.; Bhuiya, A. M.; Yu, X.; Chow, E. K.; Toussaint, K. C., Jr. Reconfigurable nanoantennas using electron-beam manipulation. *Nat. Commun.* **2014**, *5*, 4427.

(20) Tang, J.; Ou, F. S.; Kuo, H. P.; Hu, M.; Stickle, W. F.; Li, Z.; Williams, R. S. Silver-coated Si nanograss as highly sensitive surface-enhanced Raman spectroscopy substrates. *Appl. Phys. A* **2009**, *96*, 793-797.

(21) Li, Z.; Meng, G.; Huang, Q.; Hu, X.; He, X.; Tang, H.; Wang, Z.; Li, F. Ag Nanoparticle-Grafted PAN-Nanohump Array Films with 3D High-Density Hot Spots as Flexible and Reliable SERS Substrates. *Small* **2015**, *11*, 5452-5459.

(22) Men, D.; Wu, Y.; Wang, C.; Xiang, J.; Yang, G.; Wan, C.; Zhang, H. Wafer-Scale Hierarchical Nanopillar Arrays Based on Au Masks and Reactive Ion Etching for Effective 3D SERS Substrate. *Materials* **2018**, *11*.

(23) Zhao, Y.; Zhang, Y.-L.; Huang, J.-A.; Zhang, Z.; Chen, X.; Zhang, W. Plasmonic nanopillar array embedded microfluidic chips: an in situ SERS monitoring platform. *J. Mater. Chem. A* **2015**, *3*, 6408-6413.

(24) Schmidt, M. S.; Hubner, J.; Boisen, A. Large area fabrication of leaning silicon nanopillars for surface enhanced Raman spectroscopy. *Adv. Mater.* **2012**, *24*, OP11-18.

(25) Lee, M. H.; Huntington, M. D.; Zhou, W.; Yang, J. C.; Odom, T. W. Programmable soft lithography: solvent-assisted nanoscale embossing. *Nano Lett.* **2011**, *11*, 311-315.

(26) Fang, J.; Zhang, L.; Li, J.; Lu, L.; Ma, C.; Cheng, S.; Li, Z.; Xiong, Q.; You, H. A general soft-enveloping strategy in the templating synthesis of mesoporous metal nanostructures. *Nat. Commun.* **2018**, *9*, 521.

(27) Song, Y.; Xu, T.; Song, X.; Zhang, X. Integrated Microdroplets Array for Intelligent Electrochemical Fabrication. *Adv. Funct. Mater.* **2020**, 1910329.

(28) Feng, J. J.; Li, A. Q.; Lei, Z.; Wang, A. J. Low-potential synthesis of "clean" Au nanodendrites and their high performance toward ethanol oxidation. *ACS Appl. Mater. Interfaces* **2012**, *4*, 2570-2576.

(29) Tran, M.; Mundt, C.; Lan, T.; Padalkar, S. Electrodeposition of Gold Nanostructures Having Controlled Morphology. *J. Nanosci. Nanotechno.* **2018**, *18*, 3492-3498.

(30) Su, S.; Wu, Y.; Zhu, D.; Chao, J.; Liu, X.; Wan, Y.; Su, Y.; Zuo, X.; Fan, C.; Wang, L. On-Electrode Synthesis of Shape-Controlled Hierarchical Flower-Like Gold Nanostructures for Efficient Interfacial DNA Assembly and Sensitive Electrochemical Sensing of MicroRNA. *Small* **2016**, *12*, 3794-3801.

(31) Guo, S.; Wang, L.; Wang, E. Templateless, surfactantless, simple electrochemical route to rapid synthesis of diameter-controlled 3D flowerlike gold microstructure with “clean” surface. *Chem. Commun.* **2007**, 3163.

(32) Lu, S.; You, T.; Gao, Y.; Yang, N.; Zhang, C.; Yin, P. Rapid fabrication of three-dimensional flower-like gold microstructures on flexible substrate for SERS applications. *Spectrochimica Acta. A* **2019**, *212*, 371-379.

(33) Lim, D. K.; Jeon, K. S.; Kim, H. M.; Nam, J. M.; Suh, Y. D. Nanogap-engineerable Raman-active nanodumbbells for single-molecule detection. *Nat. Mater.* **2010**, *9*, 60-67.

(34) Lee, A.; Andrade, G. F.; Ahmed, A.; Souza, M. L.; Coombs, N.; Tumarkin, E.; Liu, K.; Gordon, R.; Brolo, A. G.; Kumacheva, E. Probing dynamic generation of hot-spots in self-assembled chains of gold nanorods by surface-enhanced Raman scattering. *J. Am. Chem. Soc.* **2011**, *133*, 7563-7570.

(35) Zhou, D.-L.; Wang, R.-Z.; Zhang, M.; Weng, X.; Chen, J.-R.; Wang, A.-J.; Feng, J.-J. Iron(III) ion-supported electrosynthesis of urchin-like gold arrays. *Electrochim. Acta* **2013**, *108*, 390-397.

(36) Ye, W.; Wang, D.; Zhang, H.; Zhou, F.; Liu, W. Electrochemical growth of flowerlike gold nanoparticles on polydopamine modified ITO glass for SERS application. *Electrochim. Acta* **2010**, *55*, 2004-2009.

(37) You, H.; Fang, J.; Chen, F.; Zhu, C.; Song, X.; Ding, B. Concentration profile within diffusion layer under non-forced hydrodynamic conditions measured by Michelson interferometer. *Chem. Phys. Lett.* **2008**, *465*, 131-135.

(38) You, H.; Ding, C.; Song, X.; Ding, B.; Fang, J. In situ studies of different growth modes of silver crystals induced by the concentration field in an aqueous solution. *CrystEngComm* **2011**, *13*, 4491.

(39) You, H.; Fang, J.; Chen, F.; Shi, M.; Song, X.; Ding, B. Morphological Evolution of Fractal Dendritic Silver Induced by Ions Walking within the Diffusion Layer. *J. Phys. Chem. C* **2008**, *112*, 16301-16305.

(40) Haxhimali, T.; Karma, A.; Gonzales, F.; Rappaz, M. Orientation selection in dendritic evolution. *Nat. Mater.* **2006**, *5*, 660-664.

(41) Oyama, T.; Yamaguchi, S.; Okajima, T.; Ohsaka, T.; Oyama, N. Time-differential frequency response of electrochemical quartz crystal electrode during the dissolution and deposition processes of Au in H_2SO_4 solution containing chloride ion. *J. Electroanal. Chem.* **2011**, *659*, 36-42.

(42) Lohse, S. E.; Burrows, N. D.; Scarabelli, L.; Liz-Marzán, L. M.; Murphy, C. Anisotropic Noble Metal Nanocrystal Growth: The Role of Halides. J. *Chem. Mater.* **2013**, *26*, 34-43.

(43) Langille, M. R.; Personick, M. L.; Zhang, J.; Mirkin, C. A. Defining rules for the shape evolution of gold nanoparticles. *J. Am. Chem. Soc.* **2012**, *134*, 14542-14554.

(44) Tsuji, M.; Nishio, M.; Jiang, P.; Miyamae, N.; Lim, S.; Matsumoto, K.; Ueyama, D.; Tang, X.-L. Role of chloride ions in the formation of Au@Ag core–shell nanocrystal structures by using a microwave–polyol method. *Colloids Surfaces A* **2008**, *317*, 247-255.

(45) Lv, Z.-Y.; Mei, L.-P.; Chen, W.-Y.; Feng, J.-J.; Chen, J.-Y.; Wang, A.-J. Shaped-controlled electrosynthesis of gold nanodendrites for highly selective and sensitive SERS detection of formaldehyde. *Sensors Actuat. B-Chem.* **2014**, *201*, 92-99.

(46) Wang, P.; Wu, L.; Lu, Z.; Li, Q.; Yin, W.; Ding, F.; Han, H. Gecko-Inspired Nanotentacle Surface-Enhanced Raman Spectroscopy Substrate for Sampling and Reliable Detection of Pesticide Residues in Fruits and Vegetables. *Anal. Chem.* **2017**, *89*, 2424-2431.

(47) Mao, P.; Liu, C.; Favraud, G.; Chen, Q.; Han, M.; Fratalocchi, A.; Zhang, S. Broadband single molecule SERS detection designed by warped optical spaces. *Nat. Commun.* **2018**, *9*, 5428.

(48) Zhao, W.; Xiao, S.; Zhang, Y.; Pan, D.; Wen, J.; Qian, X.; Wang, D.; Cao, H.; He, W.; Quan, M.; Yang, Z. Binary "island" shaped arrays with high-density hot spots for surface-enhanced Raman scattering substrates. *Nanoscale* **2018**, *10*, 14220-14229.

(49) Zhang, L.; Li, X.; Liu, W.; Hao, R.; Jia, H.; Dai, Y.; Usman Amin, M.; You, H.; Li, T.; Fang, J. Highly active Au NP microarray films for direct SERS detection. *J. Mater. Chem. C* **2019**, *7*, 15259-15268.

(50) Pradhan, M.; Chowdhury, J.; Sarkar, S.; Sinha, A. K.; Pal, T. Hierarchical Gold Flower with Sharp Tips from Controlled Galvanic Replacement Reaction for High Surface Enhanced Raman Scattering Activity. *J. Phy. Chem. C* **2012**, *116*, 24301-24313.

(51) Fu, R.; Liu, G.; Jia, C.; Li, X.; Tang, X.; Duan, G.; Li, Y.; Cai, W. Fabrication of silver nanoplate hierarchical turreted ordered array and its application in trace analyses. *Chem. Commun.* **2015**, *51*, 6609-6612.

(52) Fu, Z.; Shen, Z.; Fan, Q.; Hao, S.; Wang, Y.; Liu, X.; Tong, X.; Kong, X.; Yang, Z. Preparation of multi-functional magnetic–plasmonic nanocomposite for adsorption and detection of thiram using SERS. *J. Hazard. Mater.* **2020**, *392*, 122356.

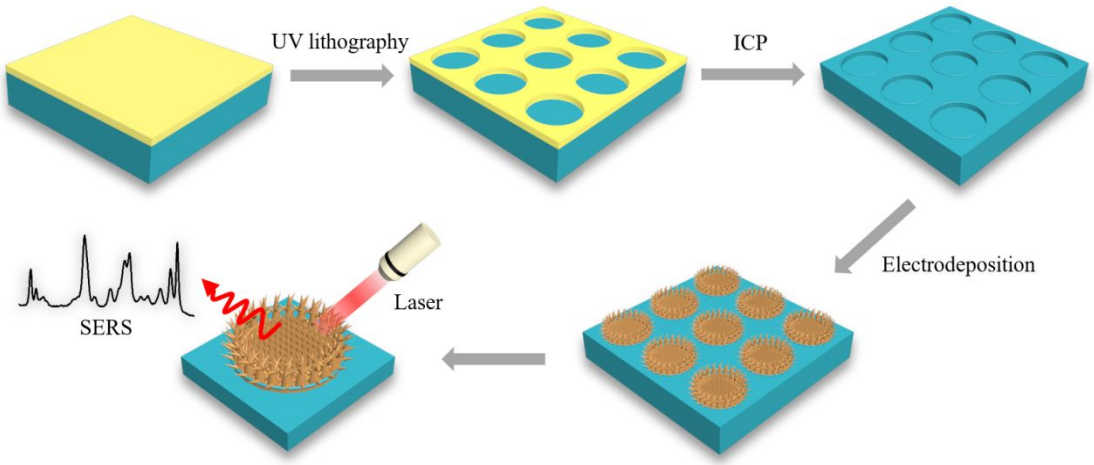

Figure 1. Schematic for the fabrication of HF-AuNTs on the Si-MP array,

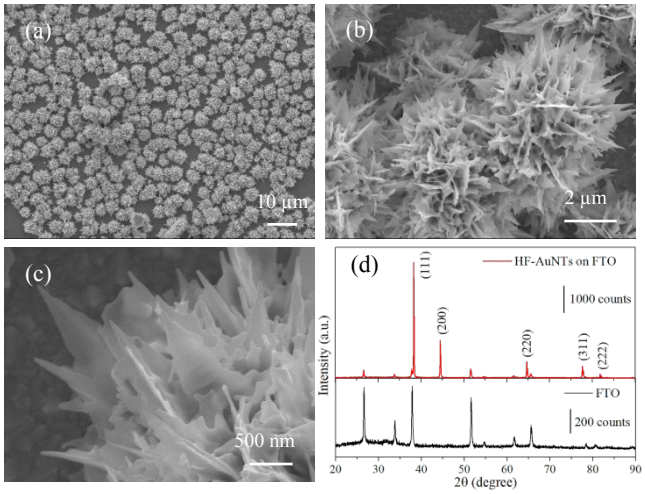

Figure 2. Typical SEM images at different magnification (a-c) and XRD spectrum (d) of HF-AuNTs on FTO surface.

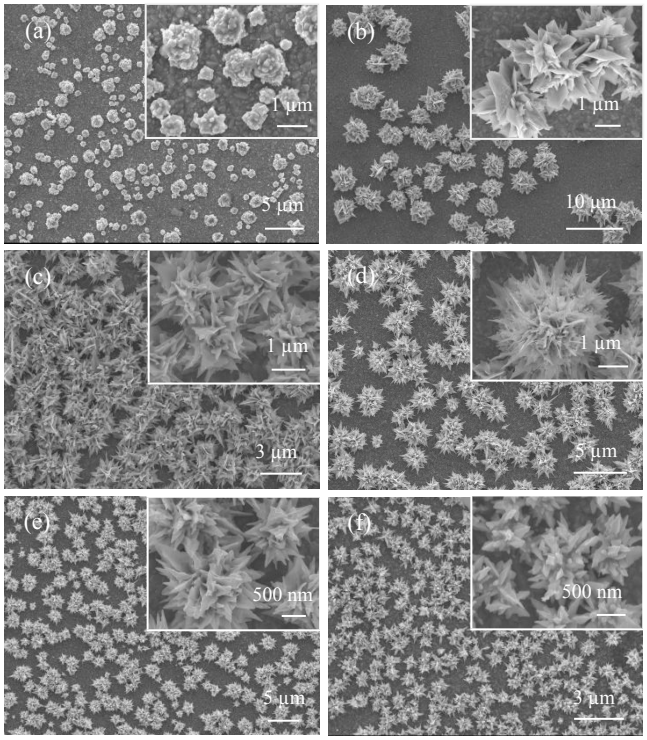

Figure 3. SEM images of gold nanostructures formed on an FTO electrode surface at different deposition potential: (a) -0.25 V, (b) -0. 5 V, (c) -0.75 V, (d) -1.0 V, (e) -1.25 V, (f) -1. 5 V in 10 mM $HAuCl_4$ and 0.5 M HCl solution for 30 min.

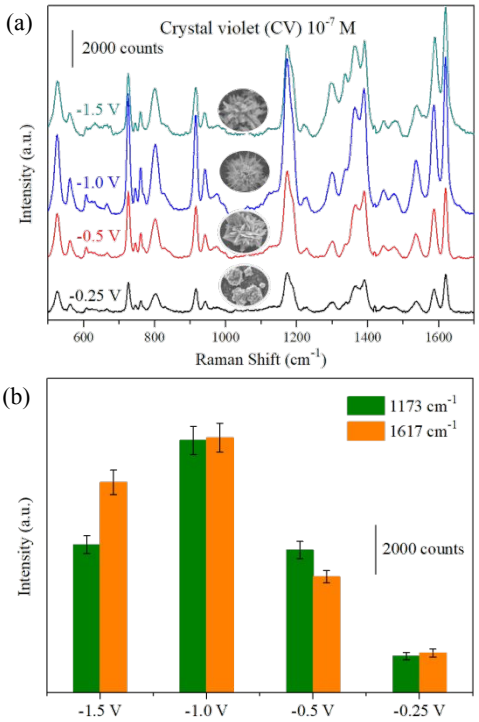

Figure 4. (a) SERS spectra of CV at 10^{-7} M from the four different Au nanostructures, (b)The peak intensity at 1173 and at 1617 cm^{-1} of CV at 10^{-7} M from the Au nanostructures at different deposition potential.

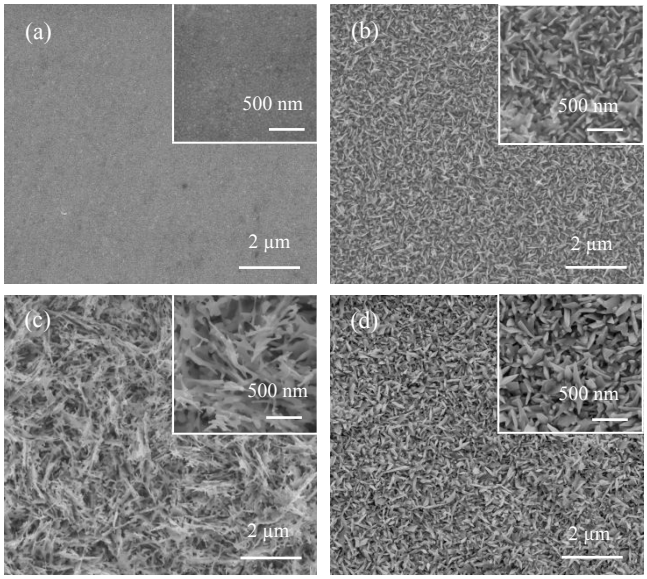

Figure 5. SEM images of electron beam evaporation Au-Si electrode (a) and gold nanostructures formed on the Au-Si electrode surface at different deposition potential: (b) -0.5 V, (c) -1.0 V, (d) -1.5 V in 10 mM $HAuCl_4$ and 0.5 M HCl solution for 30 min.

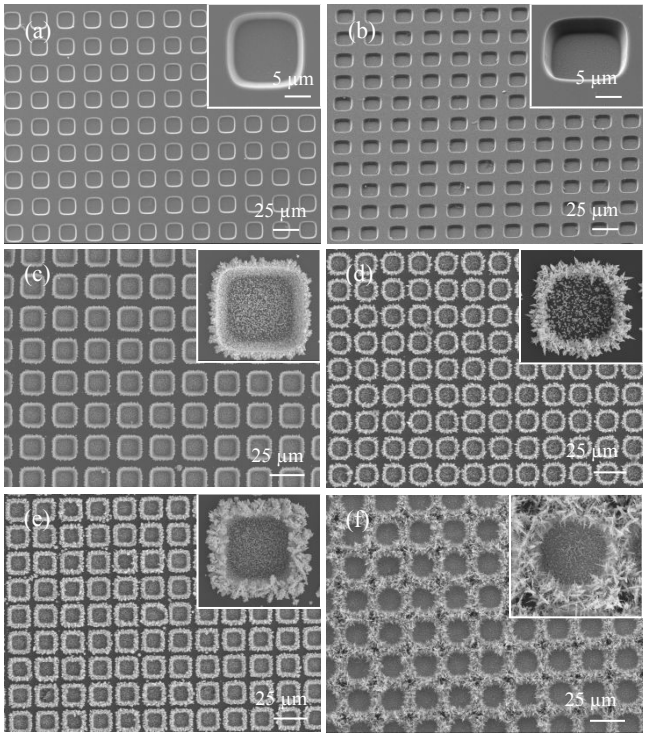

Figure 6. (a) Top view and (b) oblique view SEM images of micro-pit array. SEM images of gold nanostructures at different deposition potential: (c) -0.5 V, (d) -1.0 V, (e) -1. 5 V in 10 mM $HAuCl_4$ and 0.5 M HCl solution for 30 min and (f) -1.0 V in 10 mM $HAuCl_4$ and 0.5 M HCl solution for 60 min.

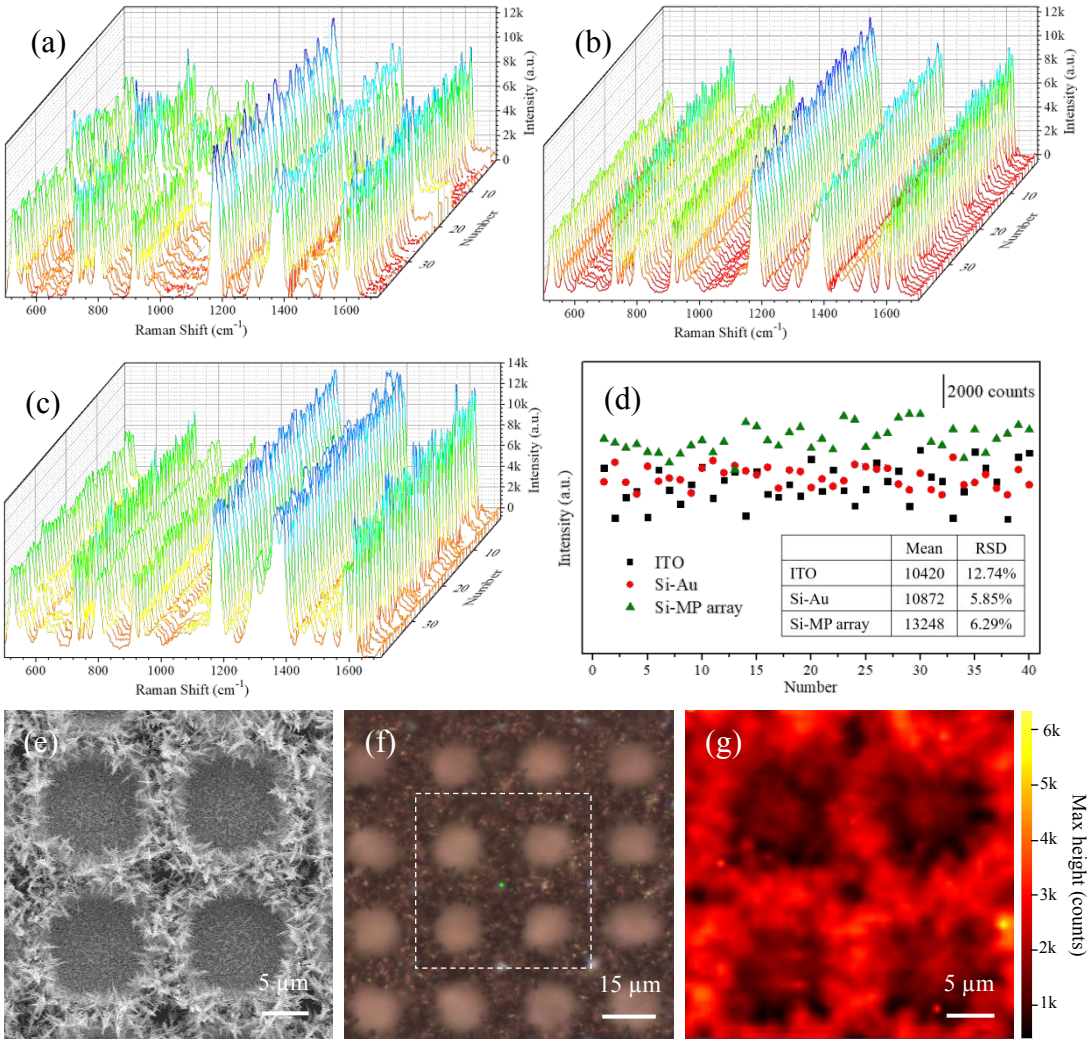

Figure 7. SERS spectra of CV with 10^{-7} M containing 40 random spots from the HF-AuNTs on the FTO (a), Si-Au (b) and Si-MP array (c) surface. (d) Intensity distribution at 1173 cm^{-1} corresponding to the SERS spectra of CV with 10^{-7} M from 40 random spots of HF-AuNTs on the FTO (black), Si-Au (red) and Si-MP array (green). (e) SEM image, (f) optical microscope image and (g) Raman micromap at 1173 cm^{-1} of HF-AuNTs microarray with 10^{-6} M CV, 1 s integration time for every step and 1 µm for step length.

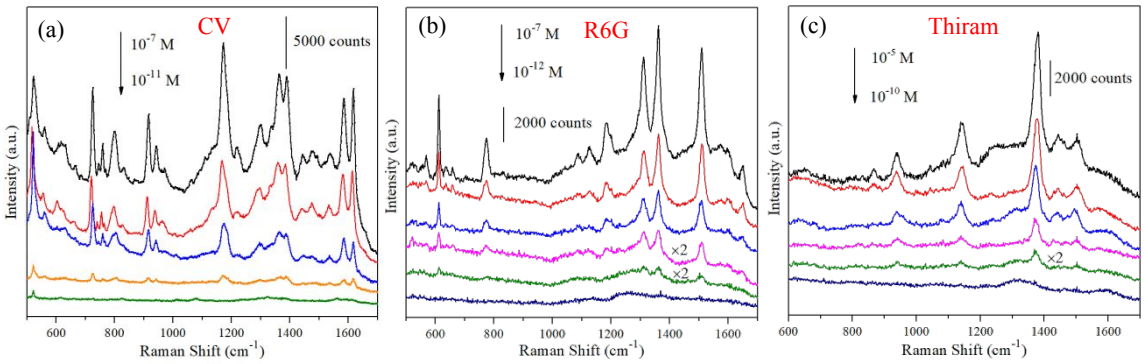

Figure 8. SERS spectra of CV from 10^{-7} to 10^{-11} M (a), R6G from 10^{-7} to 10^{-12} M (b), and thiram from 10^{-5} to 10^{-10} M (c) adsorbed on the HF-AuNTs microarray.

For Table of Contents Only